Fast whole brain imaging in adult Drosophila during response to stimuli and behavior

Sophie Aimon[1*], Takeo Katsuki[1], Logan Grosenick[2], Michael Broxton[2], Karl Deisseroth[3,4], Terrence J. Sejnowski[5,6], Ralph J. Greenspan[1,6,7]

[1] Kavli Institute for Brain and Mind, UCSD, La Jolla, CA 92093-0126, USA

[2] Departments of Computer Science and Bioengineering, Stanford University, Stanford, CA 94305, USA

[3] Departments of Bioengineering and Psychiatry, Stanford University

[4] Howard Hughes Medical Institute, Stanford University, Stanford, California, United States of America

[5] Howard Hughes Medical Institute, Computational Neurobiology Laboratory, Salk Institute for Biological Studies, La Jolla, CA 92037

[6] Division of Biological Sciences, University of California San Diego, La Jolla, CA 92093

[7] Department of Cognitive Science, University of California, San Diego, La Jolla, CA 92093

*Corresponding author: aimon.sophie@gmail.com

Abstract

Whole brain recordings give us a global perspective of the brain in action. We describe here a method using light field microscopy to record both whole brain calcium and voltage activity at high speed in behaving adult flies. We show first that global activity maps can be obtained for various stimuli and behaviors. Notably, we found that brain activity increased on a global scale when the fly walked but not when it groomed. Second, maps of spatially distinct sources of activity as well as their time series can be extracted using principal component analysis and independent component analysis. Their characteristic shapes matched the anatomy of sub-neuropil regions and in some cases a specific neuron type. Brain structures that responded to light and odor were consistent with previous reports, confirming the validity of the new technique. We also observed previously uncharacterized behavior-related activity, as well as patterns of spontaneous activity in the central complex.

Introduction

Measuring activity at the scale of the whole brain is important to understand how different brain regions interact to process and control sensory inputs, internal states and behavior. Indeed, whole brain recordings reveal which regions are involved in which functions and with what dynamics, but also help interpret the effects of a targeted intervention (such as a lesion or local excitation or inhibition with optogenetic) on the whole network, and give context to precise recordings from electrophysiology. However techniques for imaging a whole brain so far have been orders of magnitude slower than the fastest neuronal electrical activity–recent reports of whole brain fluorescence imaging in Zebrafish and Drosophila larvae immobilized in a gel had a frame rate of 12 Hz (Tomer et al., 2015) and 5 Hz (Lemon et al., 2015), respectively. A newly developed technique, light field microscopy (Broxton et al., 2013; L. Grosenick, Anderson, & Smith, 2009; L. M. Grosenick et al., 2017; Levoy, Ng, Adams, Footer, & Horowitz, 2006; Nobauer et al., 2017; Prevedel et al., 2014), makes it possible to image large volumes of scattering brain tissue at the frame rate of the fastest cameras.

Here, we leverage this technique to record large-scale activity in the brain of behaving adult fruit flies. We show that the whole brain can be imaged with a 20x objective at a frame rate up to 200 Hz, which enables the recording of the fluorescence from pan-neuronally expressed calcium (GCaMP6 (Chen et al., 2013)) or voltage (ArcLight (Jin et al., 2012)) probes. We present rich datasets of whole-brain activity along with behavior, as well as two applications of the method. First, we map whole brain activity for specific stimuli and behaviors with short time-scales. For example, we compare whole brain activity when the fly rested, walked and groomed. Second, we apply computational methods (principal component analysis: PCA, and independent component analysis: ICA) to extract components representing spatially distinct sources of activity (Beckmann & Smith, 2004; L. Grosenick et al., 2009; Mukamel, Nimmerjahn, & Schnitzer, 2009). We show that these sources correspond to sub-neuropil

53 areas or processes from small populations of neurons well characterized anatomically and compared
54 their responses to flashes of light or odor puffs with literature reports of experiments done on restricted
55 regions. Additionally, with this method we discovered neuronal projections which activity correlated
56 with turning, as well as previously unreported patterns of spontaneous activity.
57

Results

Imaging the near-whole brain of behaving adult Drosophila

We fixed a fly's head and exposed the brain while maintaining the eyes, antennae and legs intact and clean (see methods section). A ball was placed under the fly's tarsi so that it could typically rest, walk, or groom. We imaged the fly brain fluorescence using light field microscopy: as shown in Fig 1A, an upright epifluorescence microscope (equipped with a 20x NA=1.0 objective) was modified by adding a microlens array at the image plane of the objective, and placing the camera sensor at the image plane of the microlens array through relay lenses. We recorded light field images continuously with a high speed sCMOS camera up to 100 Hz for GCaMP6, or at 200 Hz using half the camera frame for ArcLight.

We then reconstructed the volumes—typically 600 x 300 x 200 μm^3 to encompass the whole brain (Fig 1B)—using the 3D deconvolution method for light field microscopy described in (ref. (Broxton et al., 2013)). Note that unlike other microscopy techniques based on scanning (e.g. two-photon, confocal or light sheet microscopy), excitation light illuminates all of the brain all the time, and all the photons emitted in the numerical aperture of the objective are used to reconstruct the image (minus a small loss through the lenses). This maximizes the number of photons collected (and thus information about brain activity) per unit of volume and time.

We measured the point spread function with 2 µm fluorescent beads embedded in a gel, and found that it widens with distance from the focal plane, varying from 3.5 to 12 µm laterally and from 6 to 35 µm axially (S1 Fig). As shown below, this resolution was sufficient to extract activity from sub-neuropil compartments.

Global activity during behavior and response to stimuli

Movie 1 and 2, Fig 2C and Fig S3C, show whole brain activity when stimuli were presented to the fly. Responses to a puff of odor and to a flash of UV light were in mostly disjoint parts of the fly brain, in accordance with previous reports in the literature: The response to light involved mostly the optic lobes, optical glomeruli and posterior slope, and the response to odor involved the antennal lobe and most of dorsal neuropils including the lateral horn, superior neuropils and the mushroom body. The global map of the response to stimuli was similar for calcium activity with GCaMP6 and voltage activity with ArcLight (FigS3C).

We also examined whole brain activity in the absence of external stimuli during spontaneous behavior which consisted of walking, grooming, and resting (see Movies 3-5). Most strikingly, the brain was more active on a global scale when the fly walked than when it rested or groomed (see Movies 3-5, Fig 2A and Fig S3A). This was observed with pan-neuronal drivers (Movie 3), but also when GCaMP6 was expressed in cholinergic neurons (most excitatory neurons in the fly brain) (Movie 4). Note that global activation during walking but very local activation during grooming is consistent with a recent large scale optogenetic study that reported that the manipulation of many region spread all over the brain altered walking but only a small region altered grooming (Robie et al., 2017)

When GCaMP6F was expressed only in dopamine neurons (Movie 5, Fig 2A and Fig S3A), we observed a strong large scale increase of activity tightly locked with walking.

Fig2B and Figure S3 show the difference in activity when the fly turned left or right. Reproducible anti-symmetrical patterns are observed in particular in the ventral regions.

Source extraction algorithm reveals functional maps at the sub-neuropil level

We applied statistical techniques, PCA and ICA, to extract maps and time series of spatially distinct sources of activity. We first aligned the brain with an anatomical template(Ito et al., 2014) using landmarks registration to automatically sort the components by brain region. We then inspected the

102 results in an interactive ipython-notebook to separate components likely due to brain activity from
103 components likely due to movement or noise (see extracts from the notebook in FigS6, FigS7, and
104 FigS8). We typically extracted a few hundred activity related components from GCaMP6 recordings and
105 50 to 100 from ArcLight recordings. Fig 3 A shows a z-stack containing all the putative activity related
106 maps (z-score>2.5) from a pan-neuronal GCaMP6 recording (see also additional flies in Fig S5), while Fig
107 3B shows the time series associated with each map (sorted by brain region). Different colors correspond
108 to different components.

109 Even though PCA and ICA are mathematical algorithms that make minimal assumption about the brain,
110 most functional maps matched well anatomical structures. In Fig 4, the left column presents a selection
111 of maps from Fig 3, or Fig S4, whereas the right column presents central complex structures from (ref
112 (Lin et al., 2013)) or neuronal processes from (ref. (Chiang et al., 2011)) assembled using Virtual Fly Brain
113 (Milyaev et al., 2012). Several sub-neuropil regions are recognizable from the shape of the maps (e.g
114 protocerebral bridge glomeruli, ellipsoid body rings and fan-shaped body layers). Note that the
115 functional maps in the fan-shaped body and the lateral horn, are the same scale as functional maps
116 obtained with higher resolution microscopy techniques ((Weir & Dickinson, 2015) and (Strutz et al.,
117 2014), respectively) suggesting that the light field microscope's resolution doesn't limit the detection of
118 relevant functional regions.

119 For some components, a neuron type could be identified from the combination of sub-neuropil regions
120 present in the map. For example, z-scored maps containing signal in one antennal lobe glomerulus, in
121 the calix, and in the lateral horn, likely arise from the activity of one type of antennal lobe projection
122 neurons. Likewise, z-scored maps with signals spanning both the horizontal and the vertical mushroom
123 body lobes likely arise from activity in alpha-beta or alpha'-beta' Kenyon cells, while maps with signal in
124 the horizontal lobe only likely arise from gamma Kenyon cells.

Extracted sources' time series retrieve known physiology in response to stimuli, and reveal projections involved in turning left or right

The component's time series were consistent with previous reports of the activity from brain structures identified in the maps, and provide new insights into the activity related to both stimuli and behavior in the same recording. Components in the optic lobe strongly responded to onset and/or offset of light (Behnia, Clark, Carter, Clandinin, & Desplan, 2014) (Fig 3); in contrast, components in the antennal lobe and the lateral horn strongly responded to the odor puffs (Wilson, 2013) (Fig S4 and Fig S6). Components likely representing the activity of antennal projection neurons were spontaneously active in the absence of odor, but their activity strongly increased with the odor (Fig S4 and Fig S6), consistent with the literature (Kazama & Wilson, 2009).

Note that the PCA and ICA algorithms helped to separate signals from artefacts such as movement or scattering from other part of the brain; however the interpretation of the time series should be made with care and compared with time series averages of the regions of interest, as the algorithm can also add some artefacts, or extract only a subpart of the neuron's activity (see Supplementary note for details about these limitations).

In addition, regions in the lateral protocerebrum, the superior slope, the antennal mechanosensory and motor center, the saddle, and the protocerebral bridge were strongly active when the fly walked (Fig 3, S4, and S8). This is consistent with previous anatomical studies as the projection from the descending neurons are most dense in the posterior slope, ventrolateral protocerebrum, and the antennal mechanosensory and motor center (Hsu & Bhandawat, 2016). Some of these walk-related components were strongly correlated with turning. As shown in Fig 5, two components per hemisphere were consistently in the components most strongly correlated with turning. The strong structural characteristics (small neuropil areas forming an inverted V shape for example, fine tracts) will help

identify candidate drivers and neurons in anatomy databases in follow up studies. Note that these components are mostly present in the posterior slope, like neurons involved in turning during flight (Suver, Huda, Iwasaki, Safarik, & Dickinson, 2016).

Restricted drivers' functional maps match single neurons anatomy

Fig 6 and S9 show components obtained when using more restrictive drivers for dopamine neurons: TH-Gal4 (same data is the same as Movie 5). As above, we sorted the components' traces and maps by brain regions (Fig 6 A). In agreement to our observation from the movie, most components were tightly correlated with the fly walking (forest green traces interleaved with the components' traces). Some of the maps in Fig 6A are reproduced in Fig 6B along with maps of single neurons from the Virtual Fly Brain database, obtained with help from automatically retrieving neuron projecting to the areas present in the maps. Some maps had unequivocal anatomical counterparts. For example, the first two maps matched well with the anatomy of processes from dopaminergic PPL1 neurons innervating mushroom body alpha lobe compartments, each component thus corresponding to only one or two cells per hemisphere (Aso et al., 2014).

Voltage recordings reveal various time scales of spontaneous activity

As shown in Fig 7, Fig S10, and Fig S11, voltage recordings with ArcLight also gave rise to maps portraying specific neuropils. Even though these data were recorded in a single trial, the time series signal to noise ratio was high enough to detect clear graded potentials–e.g. components in the optic lobe in response to onset and offset of flashes of light, and spikes-like signals–e.g. spontaneous activity and odor response for components in the antennal lobe, calix and lateral horn, consistent with the literature (Wilson, 2013), (Behnia et al., 2014).

Spike-like signals were particularly clear in a more restricted driver for dopamine and serotonin neurons (TH-Gal4 and DDC-Gal4) as shown in Fig S8. Note that the ability to record membrane voltage signals in

171 the actual neuronal processes (Cao et al., 2013; Gong et al., 2015; Yang et al., 2016) performing the
172 computation is an advantage over patch clamp experiments, which can only be recorded from the cell
173 body at the periphery of the brain in Drosophila, and thus may not be representative of the activity in
174 the neuronal processes (Gouwens & Wilson, 2009).

175 Previously unreported patterns of activity were also detected. Note, for example, the spontaneous slow
176 flip-flop activity for components in a nodulus and contralateral protocerebral bridge (Fig8, see also Fig 7,
177 second to last region and Fig S10 second and third traces). Although the fly wasn't walking in some of
178 these experiments, the maps were similar to the pattern of expression of genetic drivers known to be
179 involved in the fly's handedness (Buchanan, Kain, & de Bivort, 2015). The time series resembled the flip
180 flop pattern measured in the moth with intracellular recordings from neurons in the lateral accessory
181 lobe (Namiki, Iwabuchi, Pansopha Kono, & Kanzaki, 2014), which is directly connected with the
182 protocerebral bridge (Lin et al., 2013). Other patterns of spontaneous activity included oscillations in the
183 antennal lobe and fast ongoing activity in the ellipsoid body rings and the protocerebral bridge (see Fig
184 S10 for another experiment in which many time scales of spontaneous activity are present at the same
185 time). More work is needed to establish the conditions and consistency of these patterns of activity.

186

187 **Discussion**

188 In this article, we presented a method to record fast whole brain activity in behaving flies, unique
189 datasets produced by the method, and two examples of applications that highlight the advantages of
190 this technique. First, we showed that the technique can characterize global state changes correlated
191 with stimuli and behavior. In particular, when looking at global activity in response to stimuli from
192 different modalities, we obtained activity increases in brain regions known to be involved in processing
193 these stimuli. Furthermore, we found a more global pattern of activation when the fly walked compared

194 to when it rested or groomed. This activation could be mediated by neuromodulators, and we indeed
195 found that most dopamine neurons were silent during rest or groom, while many of these neurons
196 distributed over the whole brain were active during walking. Second, we used a blind source separation
197 algorithm to extract spatially distinct sources of activity. These sources matched anatomical sub-
198 neuropil regions, and thus helped identify neuron classes and sometimes a specific neuron type involved
199 in specific stimuli processing or behavior, but also spontaneously active in the absence of changing
200 stimuli and behavior. The datasets (available on CNCRS.org) of whole brain imaging and behavior
201 contain additional, unexplored patterns of activity and other analysis techniques will be required to
202 extract all meaningful information.

203 Although we could image the whole brain with a frame rate of 200 Hz, the time response of the probe
204 we used in this study is slower (rise time to spike peak of ~0.15 s for GCaMP6F and ~0.1 s for ArcLight in
205 our hands). Fast activity (for example at the onset of stimulus response) can still be detected, but the
206 probe's response imposes a temporal filter on the underlying activity. Deconvolution methods as well as
207 faster probes will help take full advantage of the technique's speed. This will help bridge the gap
208 between the current fast local methods using microelectrodes (recording spikes and fast oscillations),
209 and slower large scale methods such as calcium imaging.

210 Despite some limitations (see also Supplementary Note), the methods presented here can be used as a
211 functional screen to identify brain regions and neurons involved in processing any stimulus or behavior
212 that the fly can perform under the microscope–which greatly increases the range of experiments that
213 are possible compared to immobilized Zebrafish and Drosophila larvae. Furthermore, complementary to
214 screens using activation or silencing of specific neurons, the voxels and component's time series give
215 insight into the dynamics of the network, including ongoing spontaneous activity. This will help us
216 understand how the brain accomplishes various functions, in particular those involving circuit loops,

such as integrating stimuli with various types of memory to guide behavior (Aso et al., 2014) and situating the animal in space (Lin et al., 2013; Seelig & Jayaraman, 2015).

222 # Methods

223 **Fly rearing and preparation for imaging**

224 The fly genotype was as described in Supplementary Table 1, and fly stocks were obtained from the
225 Drosophila Bloomington Stock Center, Bloomington, IN. Flies were reared at 25 ^{o}C with a 24 h light/dark
226 cycle on brown food (containing cornmeal, molasses, yeast, soy flour, agar, proprionate and nipogen) as
227 it had a lower auto-fluorescence than yellow food (such as the one from the Bloomington Stock Center
228 that contains yellow cornmeal, malt extract, corn syrup, yeast, soy flour, agar and proprionic acid).

229 Fly holders were 3D printed using Supplementary data chamber.stl. A piece of tape (Scotch 3M 0.75"
230 Width) was shaped as a 1 mm high step using a 1 mm thick glass slide, and an aperture as in
231 Supplementary Figure 1 (1mm wide for the body and 0.6 mm wide for the head) was made by hand
232 using a sharpened scalpel or a thin lancet (36 gauge, TiniBoy). The tape was then stuck onto the
233 chamber, aligning the opening of the tape to the center of the holder. To block the excitation light from
234 hitting the fly's eyes, black nail polish (Black Onyx nail laquer, OPI products) was added onto the tape.
235 Nail polish was also added at the contact between the tape and the holder to avoid leaks.

236 Flies were transferred to an empty glass vial and left on ice for approximately one minute. The holder
237 was put in contact with wet tissues on ice under a stereomicroscope. A fly from the cold vial was pushed
238 into the holder’s opening so as to have the posterior part of the head in contact with the tape. UV-
239 curing glue (Fotoplast gel, Dreve), was added at the junction between the tape and the head between
240 the eyes and cured for five seconds using a 365 nm Thorlabs LED at 20% of power for 5s. A piece of thin
241 copper wire (Wire-Magnet, 40 Gauge, AmplifiedParts) or a piece of tape was placed above the legs to
242 push them away from the proboscis (see Fig 1-figure supplement 1). UV glue was then added at the rim
243 of the eye and all around the proboscis (that was pushed in the head), without touching the antenna or
244 the legs, and cured for 5s. Uncured glue was carefully removed with tissues. A small amount of vacuum

245 grease was placed around the neck behind the proboscis to avoid later leaks. The wire or tape was then
246 removed, and a small piece of tissue paper or a small styrofoam ball was given to the fly to walk on to
247 monitor its health during the following steps.

248 The holder was turned over and the fly's thorax was pushed down to clear the way to the back of the
249 brain. Small pieces of tape were added onto any remaining holes around the fly's body, and UV glue was
250 added on top of them and cured around the thorax to fix it in place. Vacuum grease was then pushed
251 towards the neck with a tissue. Saline (108 mM NaCl, 5 mM KCl, 3 mM CaCl2,4 mM MgCl2, 4 mM
252 NaHCO3, 1 mM NaH2PO4, 5 mM trehalose, 10mM sucrose, 5 mM HEPES adjusted to pH 3.35 +/- 0.05
253 with NaOH, prepared weekly) was added and left for few minutes to make sure that there were no
254 leaks.

255 Fresh saline was added and dissection was started with forceps (#5SF, Dumont) that were priorly
256 sharpened as finely as possible by hand. The cuticle in the middle of the back of the head was first
257 removed, while being careful to cut pieces before pulling them out. This exposed the hole in the middle
258 of the brain where muscle 16 resides. The pulsatile piece was pulled out. Fresh saline was added and the
259 remainder of the cuticle was removed piece by piece. The brain was washed with saline several times to
260 remove fat bodies. The air sacs were then removed very carefully to try not to displace the brain. After a
261 new wash with saline, the fly was ready for imaging.

262 **Imaging set up**

263 The microscope was modified from an upright Olympus BX51W with a 20x NA 1.0 XLUMPlanFL objective
264 (Olympus). A microlens array with pitch=125µm and f/10 to match the objective(Broxton et al., 2013)
265 (RPC Photonics), was positioned at the image plane using a custom made holder (with some parts from
266 Bioimaging Solutions, Inc). Two relay lenses (50mm f/1.4 NIKKOR-S Auto, Nikon) projected the image
267 onto the sensor of a scientific CMOS camera (Hamamatsu ORCA-Flash 4.0). A 490nm LED (pE100

268 CoolLED) at approximately 10% of its full power was used for excitation. We used a 482/25 bandpass
269 filter, a 495 nm dichroic beam splitter, and a 520/35 bandpass emission filter (BrightLine, Semrock) for
270 the fluorescence. Note that the full set up was approximately 37000 dollars (52000 dollars with the
271 64Gb of Ram acquisition computer and the 256Gb of RAM analysis computers), which is an order of
272 magnitude less than other cutting-edge microscopy techniques such as two-photon microscopes.

273 The resolution as a function of depth (see Supplementary Figure 1) was determined by imaging 2 µm
274 fluorescent beads dispersed in an agarose gel. After reconstruction, the center of beads at different
275 distances from the focal plane was recorded using ImageJ, and a Matlab program measured the half
276 height and half width of point spread function (see https://github.com/sophie63/FlyLFM for the code).

277 The fly holder was positioned on a U shaped stage above a floating ball so that the fly could walk (see
278 Figure 1 and Supplementary Videos 2 and 3). The ball was either polyurethane foam (10 mm in
279 diameter), styrofoam, or hollow HDPE (¼ inch). A cup matching the ball diameter and with a 1.2 mm
280 hole was prepared using self-curing rubber (Sugru). A bottle of compressed air provided a steady flow in
281 a pipeline consisting of a tube and a pipette tip connected to the cup hole. A micromanipulator
282 (Narishige) positioned the ball under the fly's legs. The fly and the ball were illuminated by a row of IR
283 LEDs (940nm, RaspberryPiCafe®) in the front and back of the fly, and were observed at 100 Hz using a
284 small camera (FFMV-03M2M, Point Grey).

285 For the odor stimulus, air was delivered by a pump (ActiveAQUA AAPA7.8L) through an electrically
286 controlled valve (12 Vdc Normally Closed Solenoid Valve, American Science & Surplus), bubbled in 50%
287 ethanol or 50% apple cider vinegar in a vial, and blown towards the fly through an inverted 1 mL pipette
288 tip. The valve circuit was controlled by a relay (RELAY TELECOM DPDT 2A 4.5V, Digi-Key), connected to a
289 labjack U3-HV through a LJTick-RelayDriver (LabJack). The excitation light and a 365nm or 470nm LED
290 (Thorlabs) for visual stimulation, were also triggered by the LabJack, which was controlled using Matlab

programs (see https://github.com/sophie63/FlyLFM for the code). In a typical experiment, the cameras for monitoring the behavior and the fluorescence were started first, and then the Matlab program was launched. The fluorescence images were recorded with HCImage (Hamamatsu) and streamed to RAM on a 64Gb of RAM computer, which allowed to record approximately 1 min of experiment continuously.

Analysis

The light field images were reconstructed using a program in python as described in ref. (Broxton et al., 2013). Briefly, a point spread function library corresponding to the specific set up was first generated. Then the images were reconstructed using 3D deconvolution on a cluster of GPUs (generously provided by the Qualcomm Institute at UCSD). A dataset of 10000 time steps required approximately 8 hours to reconstruct on a cluster of 15 GPUs.

The images were assembled in a Nifti file using a python routine (Tiff2niiV2 in https://github.com/sophie63/FlyLFM), inspected and cropped in FIJI, and the first 5s were discarded as the strong activity in response to the excitation light made it difficult to correct for movement and photobleaching. The 3D image registration function 3dvolreg (Cox & Jesmanowicz, 1999) from AFNI was then used to correct for movements in 3D. The background fluorescence, as well as the decrease in intensity from photobleaching, were removed by subtracting a signal smoothed using a box average over 15 to 30 s depending on the severity of the bleaching and the length of the recording. The time series were then multiplied by -1 for ArcLight data. For denoising, a Kalman filter (from https://www.mathworks.com/matlabcentral/fileexchange/26334-kalman-filter-for-noisy-movies) with a gain of 0.5 was better than a median filter over 3 points, and was used for the figures in this paper. The reconstructed data as well as the data after preprocessing will be soon available on the CRCNS website (https://crcns.org/NWB/Data_sets).

The fluorescence and the behavior were aligned using the onset and offset of the excitation light. First the small discrepancy (approximately 30 ms per min) between the total time given by the camera for the fluorescence and the camera for the behavior was corrected linearly, then the fluorescence data was interpolated to match the behavior data using the matlab function Interpolate2vid (see https://github.com/sophie63/FlyLFM). For movie 1, 2, and 3, the minimum value for each pixel was added to have all values positive. The behavior was analyzed manually (pressing different keyboard keys when different behavior were recognized) using the Matlab GUI Video_Annotate in https://github.com/sophie63/FlyLFM. The fly's walk was also characterized by tracking the movements of the ball using ImageJ's optic flow plugin (Gaussian Window MSE).

Maps comparing the activity during rest and walk, rest and groom, turning left and turning right, and one second after stimulus presentation compared to one second before were obtained by simply averaging the time series in each voxel for the different conditions, and subtracting these maps from one another. The positive value was colored in red and the negative in green thus showing which condition dominates in which voxel.

The average of the time series was aligned to an anatomical template (available here: https://github.com/VirtualFlyBrain/DrosAdultBRAINdomains) in which the brain is segmented in regions according to the nomenclature described in (Ito et al., 2014). The registration was performed using landmarks with ImageJ as described in http://imagej.net/Name_Landmarks_and_Register.

Dimensionality was then reduced by separating the volumes in slices of thickness corresponding to the point spread function height, and averaging in z for each slice. The 4D data sets were typically (x,y,z,t)=200x100x10x10000 at this stage.

PCA and ICA were applied with a Matlab code using a fast SVD algorithm and Fastica (Hyvärinen, 1999) (see ICAalamelodic.m file from https://github.com/sophie63/FlyLFM), or using melodic (Beckmann &

Smith, 2004) from the FSL package (for Fig 4-supplementary figure 1). The principal component spectrum was inspected to determine the number of components. The sign was chosen to have the average of the positive side of the map larger than the negative side. The components were then sorted by brain region, and pruning was done by hand using an interactive ipython notebook (the notebooks corresponding to the choices made for the figures in this paper can be found at https://github.com/sophie63/FlyLFM). Only the components for which the maps were localized and the time series showed distinct patterns of activity such as spikes were kept. The other components likely corresponded to movement artefacts or noise, and imposing more components for PCA and ICA typically increased the number of noise components without affecting the components corresponding to brain activity.

The time series for turning left or right were obtained by convolving the optic flow for the ball going left or right, with a kernel corresponding to the impulse response of GCaMP6. These time series were then regressed with the time series or the components, and we inspected the maps with the strongest regression coefficient.

Image manipulations

Figure 1B bar was added with ImageJ and the 3D rendering was done in Icy(de Chaumont et al., 2012), in which transparency and contrast were adjusted globally on the volume. The component's maps were thresholded at $2.5 \times \sigma$ in python (see the ipython notebooks), and only the positive part of the map is displayed. The image contrast was then adjusted globally in ImageJ and the figures were assembled in Inkscape.

Code availability

The Matlab and Python code for preprocessing, PCA/ICA and sorting of the components is available at: https://github.com/sophie63/FlyLFM.

Author Contributions

R. Greenspan and T. Katsuki had the idea of using light field microscopy to image the whole fly brain. T. Sejnowski proposed to use PCA and ICA to extract activity from the recordings. L. Grosenick, M. Broxton and K. Deisseroth provided advice and training on the light field microscopy setup, the code for 3D deconvolution, and a computational infrastructure for deconvolving large numbers of volumes. R. Greenspan and T. Sejnowski supervised the research. T. Katsuki performed early experiments and advised S. Aimon throughout the project. S. Aimon designed and performed the experiments presented in the paper and wrote the manuscript. All the authors critically reviewed the manuscript.

Acknowledgements

We thank Jürgen Schulze, Joseph Keefe and Calit2 for generously providing a GPU cluster. Charles F. Stevens contributed many helpful discussions and comments on the manuscript. Angelique Paulk provided valuable advices on the floating ball set-up. Stephen M. Smith helped with reproducing parts of melodic in Matlab, Ryan Shultzaberger helped with R and bash, and Nicolas Aimon helped with fitting time series in python. M. Nitabach and V. Pieribone gave us UAS-Arclight flies and the Nitabach laboratory provided technical support on imaging Arclight.

Aso, Y., Hattori, D., Yu, Y., Johnston, R. M., Iyer, N. A., Ngo, T.-T. T., … Rubin, G. M. (2014). The neuronal architecture of the mushroom body provides a logic for associative learning. *eLife*, *3*, 1–48. https://doi.org/10.7554/eLife.04577

Beckmann, C. F., & Smith, S. M. (2004). Probabilistic independent component analysis for functional magnetic resonance imaging. *IEEE Transactions on Medical Imaging*, *23*(2), 137–52. https://doi.org/10.1109/TMI.2003.822821

Behnia, R., Clark, D. A., Carter, A. G., Clandinin, T. R., & Desplan, C. (2014). Processing properties of ON and OFF pathways for Drosophila motion detection. *Nature*, *512*(7515), 427–30. https://doi.org/10.1038/nature13427

Broxton, M., Grosenick, L., Yang, S., Cohen, N., Andalman, A., Deisseroth, K., & Levoy, M. (2013). Wave optics theory and 3-D deconvolution for the light field microscope. *Optics Express*, *21*(21), 25418–39. https://doi.org/10.1364/OE.21.025418

Buchanan, S. M., Kain, J. S., & de Bivort, B. L. (2015). Neuronal control of locomotor handedness in Drosophila. *Proceedings of the National Academy of Sciences of the United States of America*, *112*(21), 6700–5. Retrieved from http://www.pnas.org/content/112/21/6700.abstract

Cao, G., Platisa, J., Pieribone, V. A., Raccuglia, D., Kunst, M., & Nitabach, M. N. (2013). Genetically targeted optical electrophysiology in intact neural circuits. *Cell*, *154*(4), 904–913. https://doi.org/10.1016/j.cell.2013.07.027

Chen, T.-W., Wardill, T. J., Sun, Y., Pulver, S. R., Renninger, S. L., Baohan, A., … Kim, D. S. (2013). Ultrasensitive fluorescent proteins for imaging neuronal activity. *Nature*, *499*(7458), 295–300. https://doi.org/10.1038/nature12354

Chiang, A.-S., Lin, C.-Y., Chuang, C.-C., Chang, H.-M., Hsieh, C.-H., Yeh, C.-W., … Hwang, J.-K. (2011). Three-dimensional reconstruction of brain-wide wiring networks in Drosophila at single-cell

resolution. *Current Biology : CB*, *21*(1), 1–11. https://doi.org/10.1016/j.cub.2010.11.056

Cox, R. W., & Jesmanowicz, a. (1999). Real-time 3D image registration for functional MRI. *Magnetic Resonance in Medicine*, *42*, 1014–1018. https://doi.org/10.1002/(sici)1522-2594(199912)42:6<1014::aid-mrm4>3.0.co;2-f

de Chaumont, F., Dallongeville, S., Chenouard, N., Hervé, N., Pop, S., Provoost, T., … Olivo-Marin, J.-C. (2012). Icy: an open bioimage informatics platform for extended reproducible research. *Nature Methods*, *9*(7), 690–6. https://doi.org/10.1038/nmeth.2075

Gong, Y., Huang, C., Li, J. Z., Grewe, B. F., Zhang, Y., Eismann, S., & Schnitzer, M. J. (2015). High-speed recording of neural spikes in awake mice and flies with a fluorescent voltage sensor. *Sciencexpress*, (November), 1–11. https://doi.org/10.1126/science.aab0810

Gouwens, N. W., & Wilson, R. I. (2009). Signal propagation in Drosophila central neurons. *The Journal of Neuroscience : The Official Journal of the Society for Neuroscience*, *29*(19), 6239–49. https://doi.org/10.1523/JNEUROSCI.0764-09.2009

Grosenick, L., Anderson, T., & Smith, S. J. (2009). Elastic Source Selection for in vivo imaging of neuronal ensembles. In *Proceedings IEEE International Symposium on Biomedical Imaging: From nano to macro* (pp. 6–9). https://doi.org/10.1109/ISBI.2009.5193292

Grosenick, L. M., Broxton, M., Kim, C. K., Liston, C., Poole, B., Yang, S., … Deisseroth, K. (2017). Identification Of Cellular-Activity Dynamics Across Large Tissue Volumes In The Mammalian Brain. *bioRxiv*. Retrieved from http://biorxiv.org/content/early/2017/05/01/132688.abstract

Hsu, C. T., & Bhandawat, V. (2016). Organization of descending neurons in Drosophila melanogaster. *Scientific Reports*, *6*, 20259. https://doi.org/10.1038/srep20259

Hyvärinen, A. (1999). Fast and robust fixed-point algorithms for independent component analysis. *IEEE Transactions on Neural Networks / a Publication of the IEEE Neural Networks Council*, *10*(3), 626–

34. https://doi.org/10.1109/72.761722

Ito, K., Shinomiya, K., Ito, M., Armstrong, J. D., Boyan, G., Hartenstein, V., … Vosshall, L. B. (2014). A systematic nomenclature for the insect brain. *Neuron*, *81*(4), 755–765. https://doi.org/10.1016/j.neuron.2013.12.017

Jin, L., Han, Z., Platisa, J., Wooltorton, J. R. A., Cohen, L. B., & Pieribone, V. A. (2012). Single Action Potentials and Subthreshold Electrical Events Imaged in Neurons with a Fluorescent Protein Voltage Probe. *Neuron*, *75*(5), 779–785. https://doi.org/10.1016/j.neuron.2012.06.040

Kazama, H., & Wilson, R. I. (2009). Origins of correlated activity in an olfactory circuit. *Nature Neuroscience*, *12*(9), 1136–1144. https://doi.org/10.1038/nn.2376

Lemon, W. C., Pulver, S. R., Hockendorf, B., McDole, K., Branson, K., Freeman, J., & Keller, P. J. (2015). Whole-central nervous system functional imaging in larval Drosophila. *Nat Commun*, *6*. Retrieved from http://dx.doi.org/10.1038/ncomms8924

Levoy, M., Ng, R., Adams, A., Footer, M., & Horowitz, M. (2006). Light field microscopy. *ACM Transactions on Graphics*, *25*(3), 924. https://doi.org/10.1145/1141911.1141976

Lin, C. Y., Chuang, C. C., Hua, T. E., Chen, C. C., Dickson, B. J., Greenspan, R. J., & Chiang, A. S. (2013). A Comprehensive Wiring Diagram of the Protocerebral Bridge for Visual Information Processing in the Drosophila Brain. *Cell Reports*, *3*(5), 1739–1753. https://doi.org/10.1016/j.celrep.2013.04.022

Milyaev, N., Osumi-sutherland, D., Reeve, S., Burton, N., Baldock, R. a., & Armstrong, J. D. (2012). The virtual fly brain browser and query interface. *Bioinformatics*, *28*(3), 411–415. https://doi.org/10.1093/bioinformatics/btr677

Mukamel, E. A., Nimmerjahn, A., & Schnitzer, M. J. (2009). Automated analysis of cellular signals from large-scale calcium imaging data. *Neuron*, *63*(6), 747–760. Retrieved from http://www.ncbi.nlm.nih.gov/pubmed/19778505

Namiki, S., Iwabuchi, S., Pansopha Kono, P., & Kanzaki, R. (2014). Information flow through neural circuits for pheromone orientation. *Nature Communications*, *5*, 5919. https://doi.org/10.1038/ncomms6919

Nobauer, T., Skocek, O., Pernia-Andrade, A. J., Weilguny, L., Traub, F. M., Molodtsov, M. I., & Vaziri, A. (2017). Video rate volumetric Ca2+ imaging across cortex using seeded iterative demixing (SID) microscopy. *Nat Meth*, *advance on*. Retrieved from http://dx.doi.org/10.1038/nmeth.4341

Prevedel, R., Yoon, Y.-G., Hoffmann, M., Pak, N., Wetzstein, G., Kato, S., … Vaziri, A. (2014). Simultaneous whole-animal 3D imaging of neuronal activity using light-field microscopy. *Nature Methods*, *11*(7), 727–30. https://doi.org/10.1038/nmeth.2964

Robie, A. A., Hirokawa, J., Edwards, A. W., Simpson, J. H., Reiser, M. B., Branson, K., … Branson, K. (2017). Mapping the Neural Substrates of Behavior Resource Mapping the Neural Substrates of Behavior. *Cell*, *170*(2), 393–406.e28. https://doi.org/10.1016/j.cell.2017.06.032

Seelig, J. D., & Jayaraman, V. (2015). Neural dynamics for landmark orientation and angular path integration. *Nature*, *521*(7551), 186–191. https://doi.org/10.1038/nature14446

Strutz, A., Soelter, J., Baschwitz, A., Farhan, A., Grabe, V., Rybak, J., … Sachse, S. (2014). Decoding odor quality and intensity in the Drosophila brain. *eLife*, *3*, e04147. https://doi.org/10.7554/eLife.04147

Suver, M. P., Huda, A., Iwasaki, N., Safarik, S., & Dickinson, M. H. (2016). An Array of Descending Visual Interneurons Encoding Self-Motion in Drosophila. *Journal of Neuroscience*, *36*(46). Retrieved from http://www.jneurosci.org/content/36/46/11768.long

Tomer, R., Lovett-Barron, M., Kauvar, I., Andalman, A., Burns, V. M., Sankaran, S., … Deisseroth, K. (2015). SPED Light Sheet Microscopy: Fast Mapping of Biological System Structure and Function. *Cell*, *163*(7), 1796–1806.

Weir, P. T., & Dickinson, M. H. (2015). Functional divisions for visual processing in the central brain of

flying Drosophila. *Proceedings of the National Academy of Sciences of the United States of America*, *112*(40), E5523-32. https://doi.org/10.1073/pnas.1514415112

Wilson, R. I. (2013). Early olfactory processing in Drosophila: mechanisms and principles. *Annual Review of Neuroscience*, *36*, 217–41. https://doi.org/10.1146/annurev-neuro-062111-150533

Yang, H. H. H., St-Pierre, F., Sun, X., Ding, X., Lin, M. Z. Z., & Clandinin, T. R. R. (2016). Subcellular Imaging of Voltage and Calcium Signals Reveals Neural Processing In??Vivo. *Cell*, *166*(1), 245–257. https://doi.org/10.1016/j.cell.2016.05.031

Figure 1: Imaging the fly brain using light field microscopy. A) Experimental set up. The fly is head fixed and its tarsi are touching a ball. The light from the brain goes through the objective, the microscope tube lens, a microlens array, and relay lenses, onto the sensor of a high-speed sCMOS camera. The behavior is recorded with another camera in front of the fly. B) Example of a light field deconvolution. Top: 2D light field image acquired in 5ms with a 20x NA 2.0 objective. Bottom: Anterior and posterior views (slightly tilted sideways) of the computationally reconstructed volume. 3D bar is 90x30x30 microns. See also Fig S1.

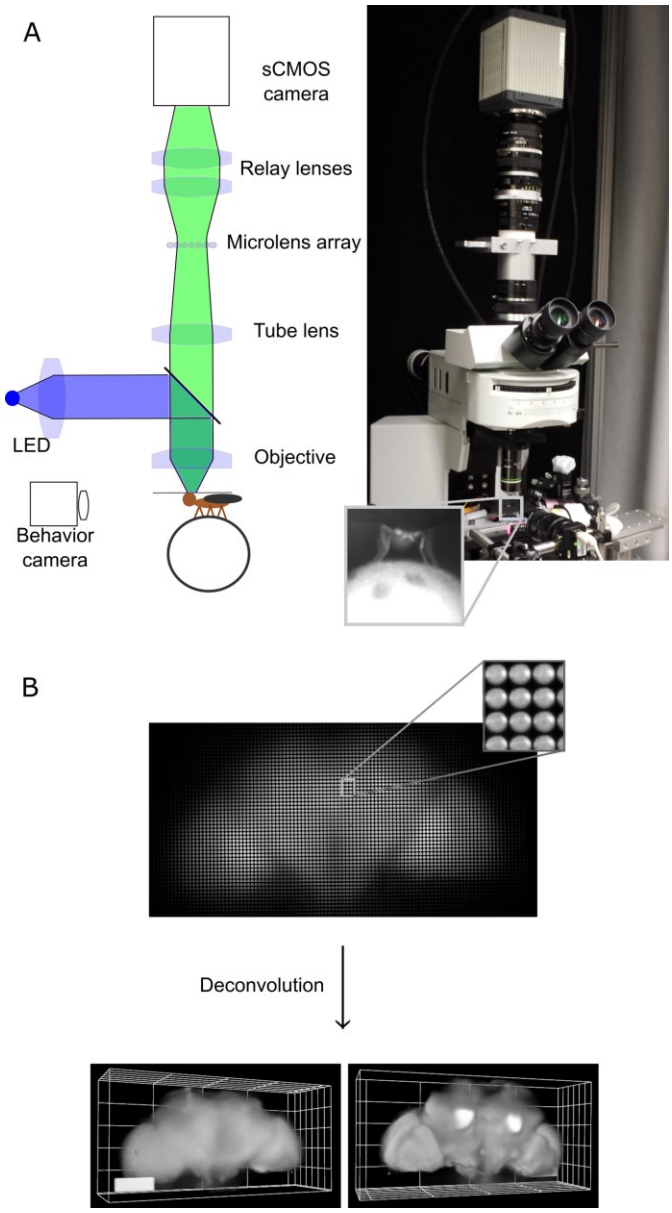

Figure 2: Whole brain activity maps for various conditions. A) Comparison of fluorescence intensity when the fly rests and when it is active (either walk of groom). The pixel value is green if the fluorescence is higher during the behavior, magenta if the fluorescence is higher during rest. B) Comparison of fluorescence intensity when the fly turns left or right. C) Comparison of fluorescence increase during the response to stimuli for odor (magenta), and light (green). See also Fig S2.

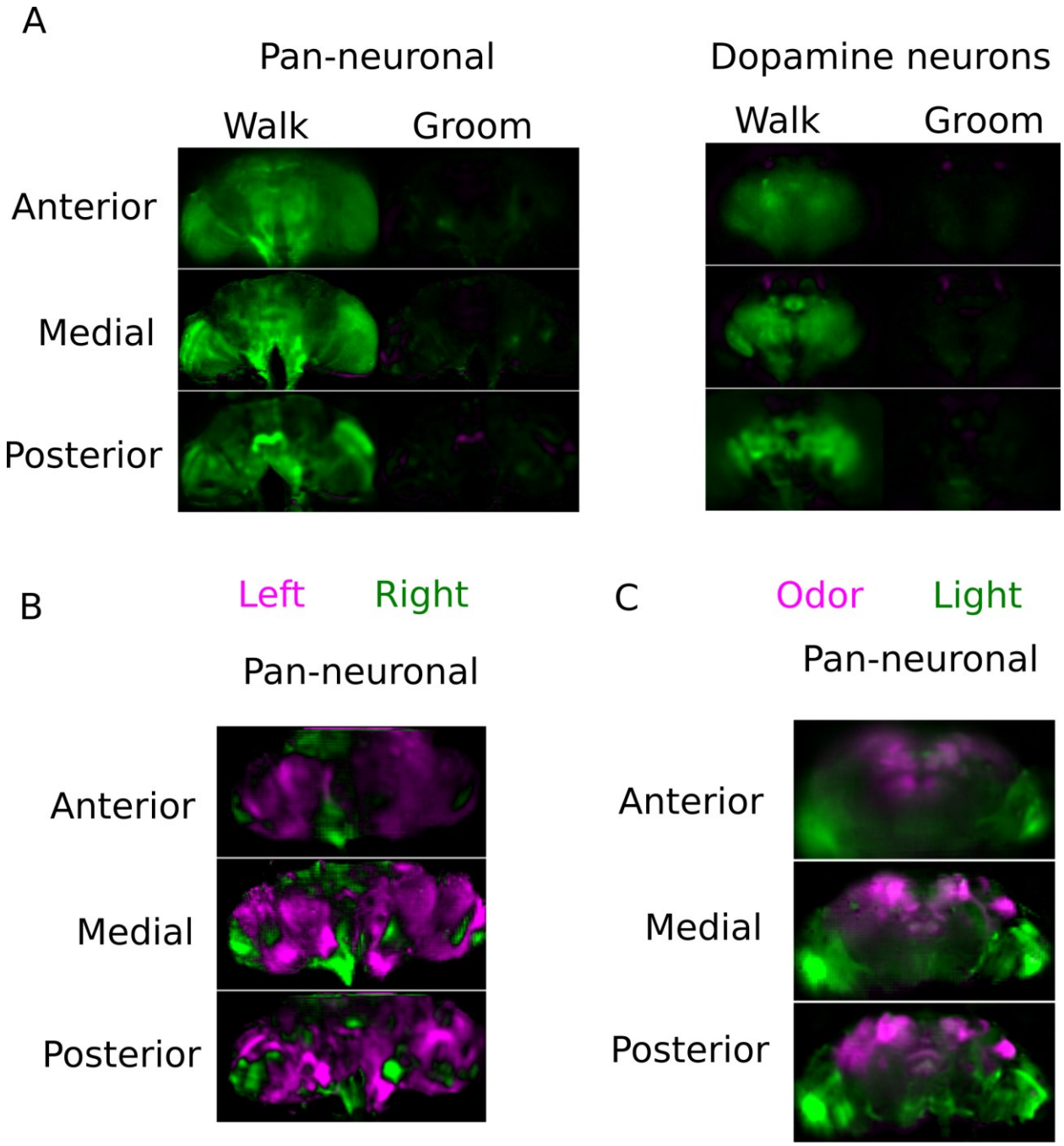

496 Figure 3: Z-scored maps and time series of the sources extracted using PCA and ICA for an experiment in
497 which flashes of UV light were presented to a fly expressing GCaMP6f pan-neuronally. A) Z-stack of the
498 3D map. Different colors correspond to different components. B) Time series (left) associated with the
499 maps (right) sorted by brain regions and projected along the z axis. Flashes of UV light are indicated in
500 purple, and the moments when the fly walks are in forest green (in gray is a time period during which
501 the fly's behavior was unclear). Bar: 90µm. See also Fig S3, S4, and S5.

502

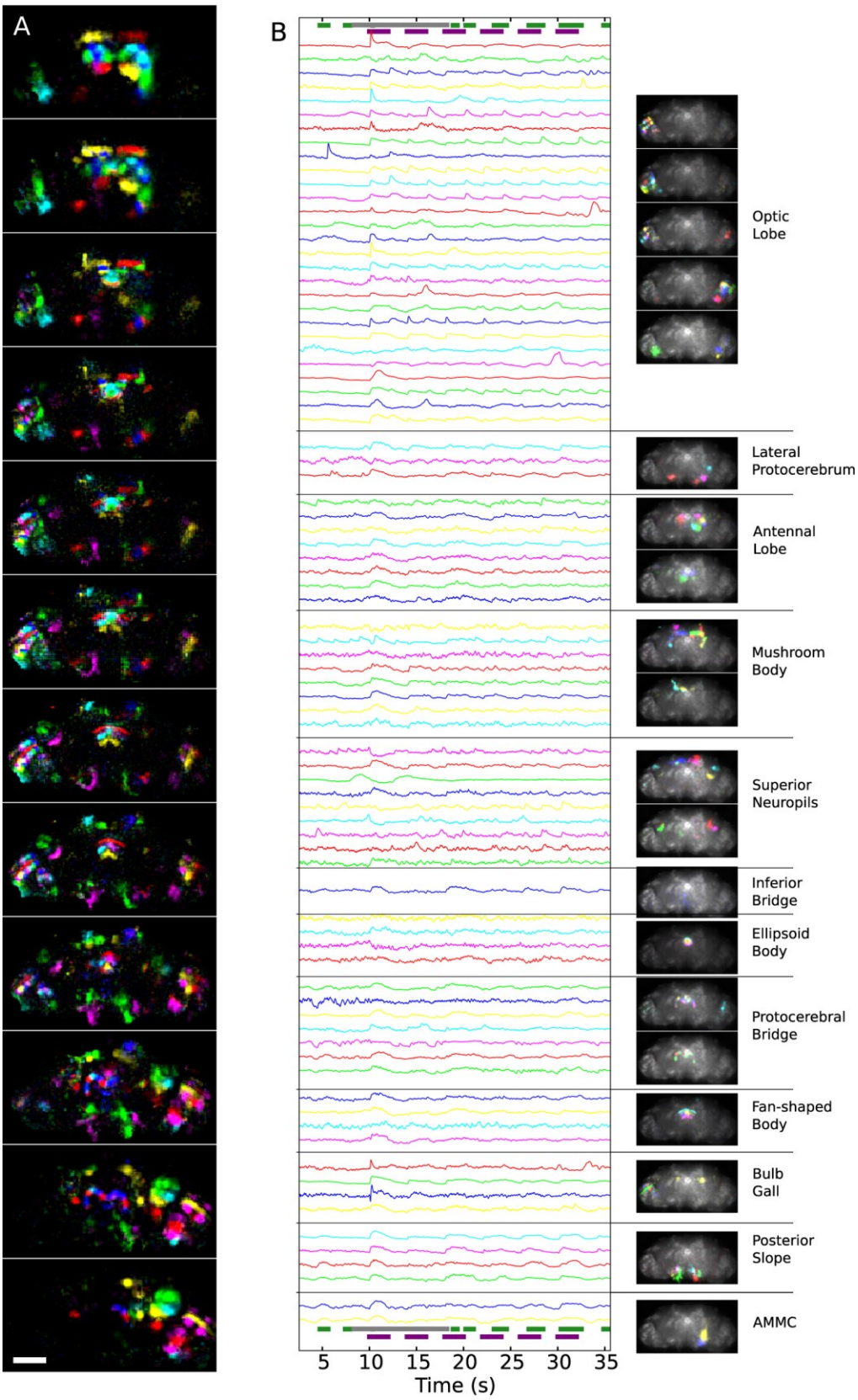
A
B
Optic Lobe
Lateral Protocerebrum
Antennal Lobe
Mushroom Body
Superior Neuropils
Inferior Bridge
Ellipsoid Body
Protocerebral Bridge
Fan-shaped Body
Bulb Gall
Posterior Slope
AMMC
5 10 15 20 25 30 35
Time (s)

503

Figure 4: Comparison between functional and anatomical maps. Left: functional maps chosen from Fig 2 and Fig S2. Right: corresponding anatomical structures. Top three images correspond to central complex structures–modified from Cell Reports, Vol. 3, Lin, C. Y. et al.,“ A Comprehensive Wiring Diagram of the Protocerebral Bridge for Visual Information Processing in the Drosophila Brain.,” 1739-1753, Copyright 2013, with permission from Elsevier, and four bottom images were neurons chosen in the Virtual Fly Brain database.

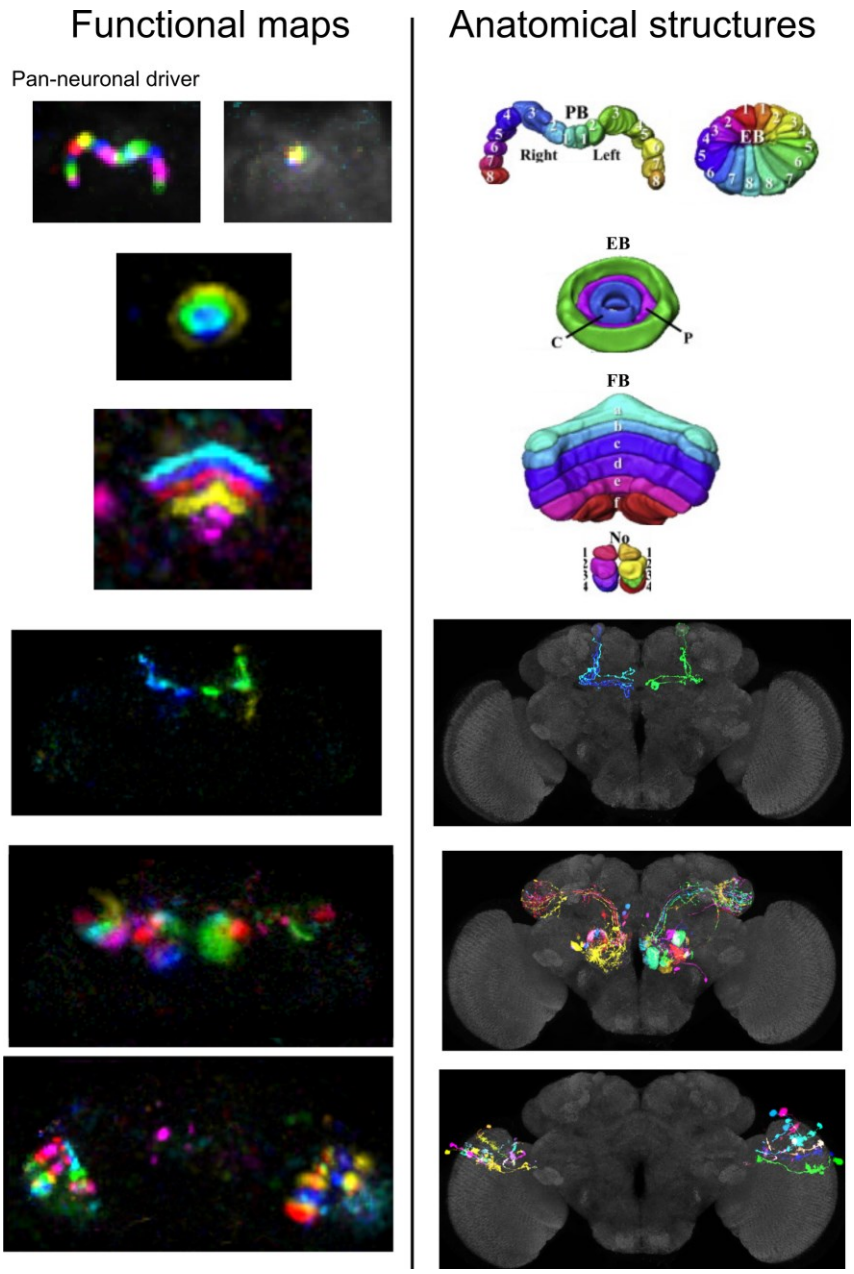

Figure 5: Zstacks of components from the most correlated to turning left (mixes of red and green) and right (mixes of blue and green). One color corresponds to one component. Flies expressed GCaMP6 pan-neuronally. Note that different flies have slightly different brain orientation.

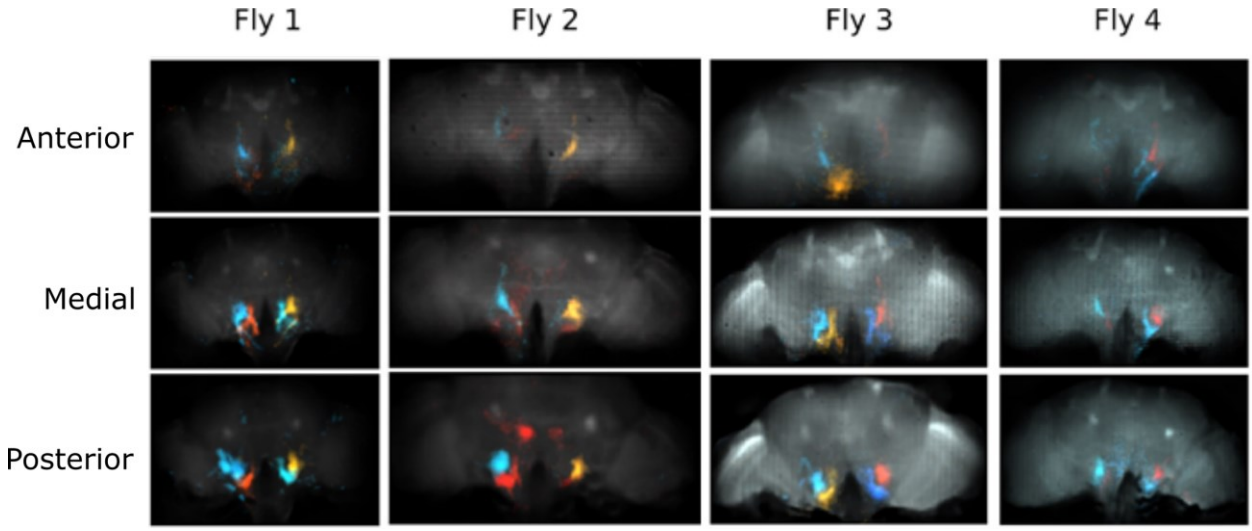

Figure 6: Components from flies expressing GCaMP6F in dopamine and neurons. A) All activity-related components are presented and sorted by brain region, with the color of the time series on the left matching the color of the maps on the right. Note that most components are strongly correlated with the fly walking (forest green traces interleaved with the component traces). The fly was resting or grooming the rest of the time. B) Example of single neuron anatomy from the VFB database (right) matching the components' maps (left). See also Fig S6.

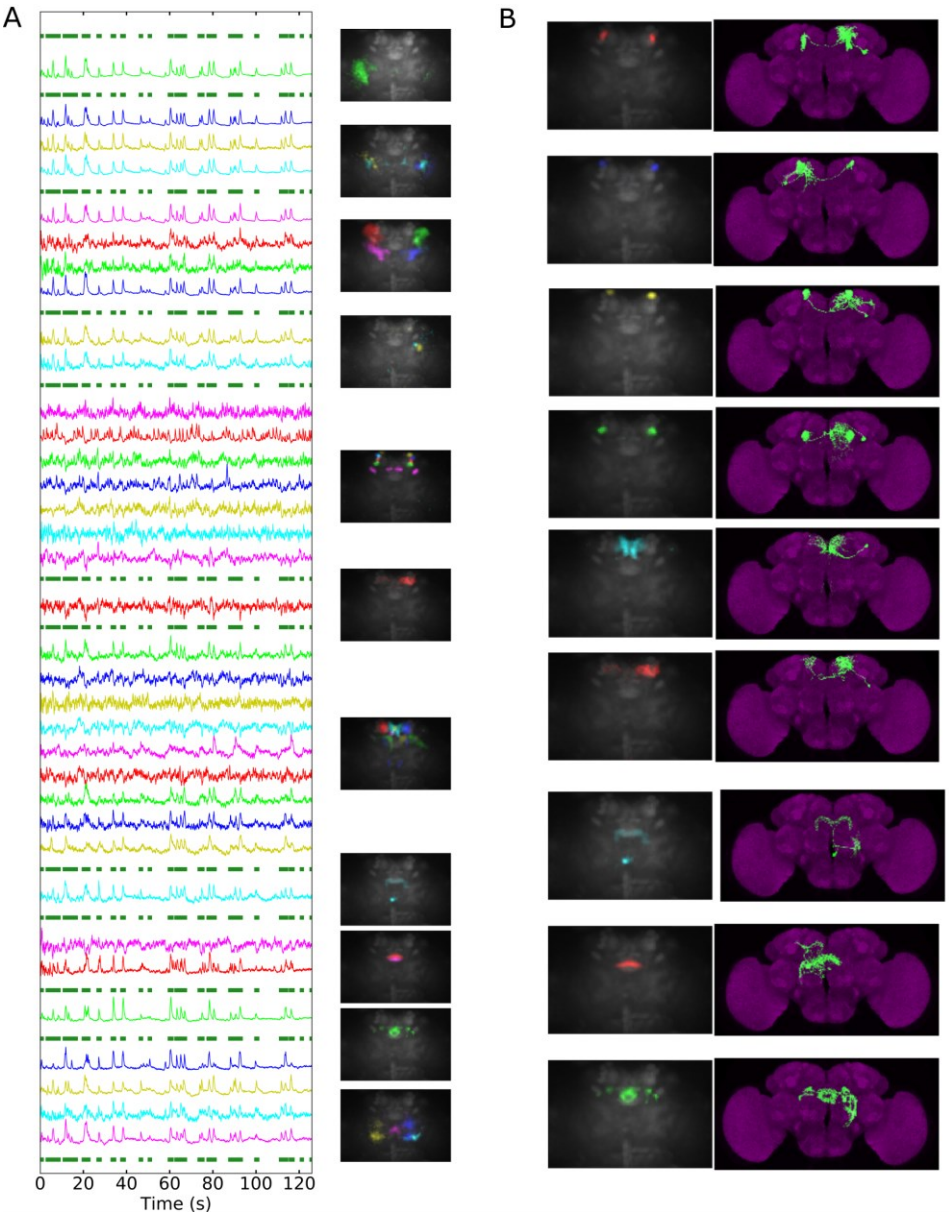

Figure 7: Components extracted from whole brain voltage activity. Arclight was expressed pan-neuronally (nSyb-GAL4). The fly was presented periodic flashes of UV light (violet bars) and puffs of apple cider vinegar (pink bars). Shown on the left are the component time series, while on the right are the corresponding maps (PB: protocerebral bridge, FB: fan-shaped body), sorted by the brain region majorly present in the map. See also Fig S7 and S8.

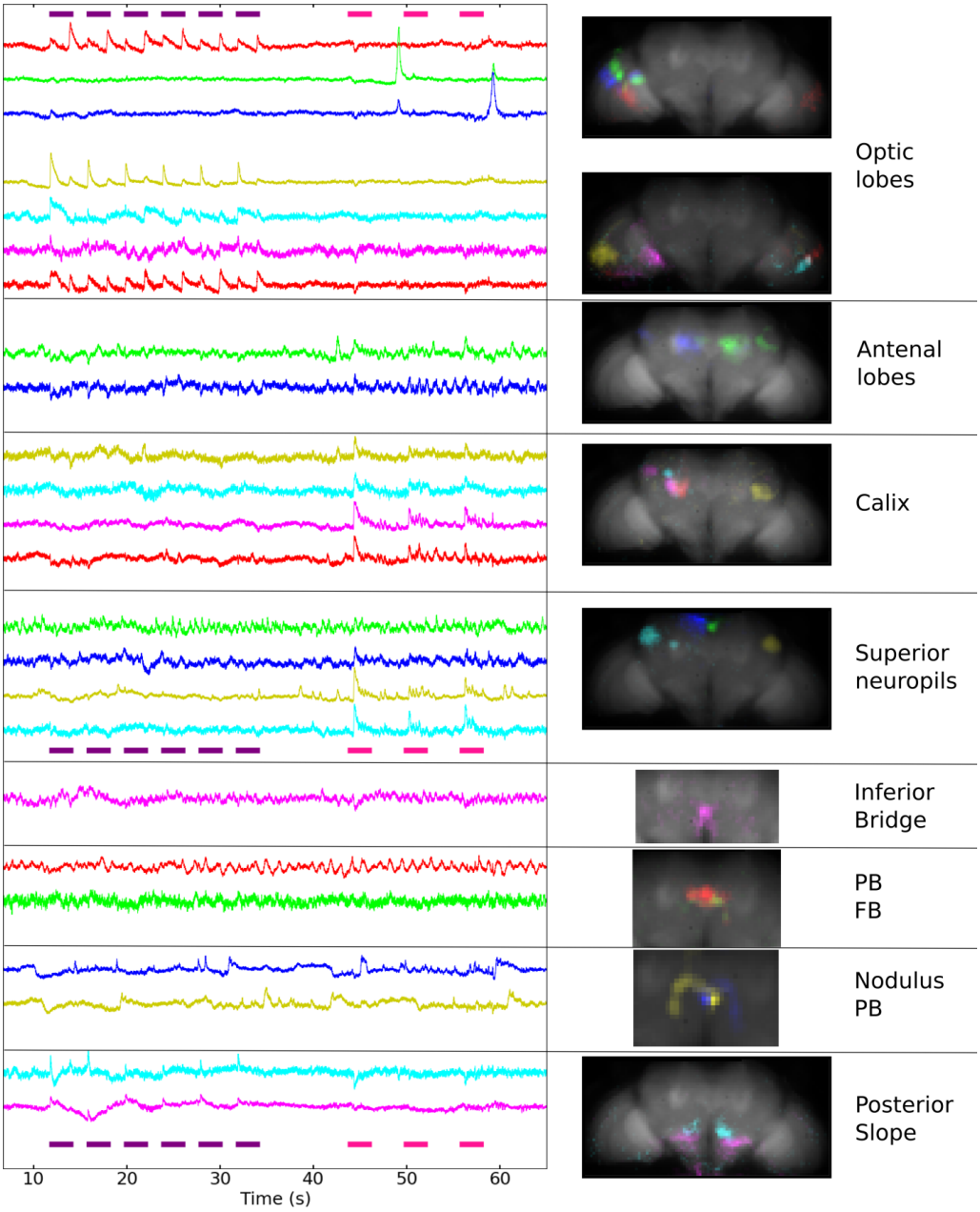
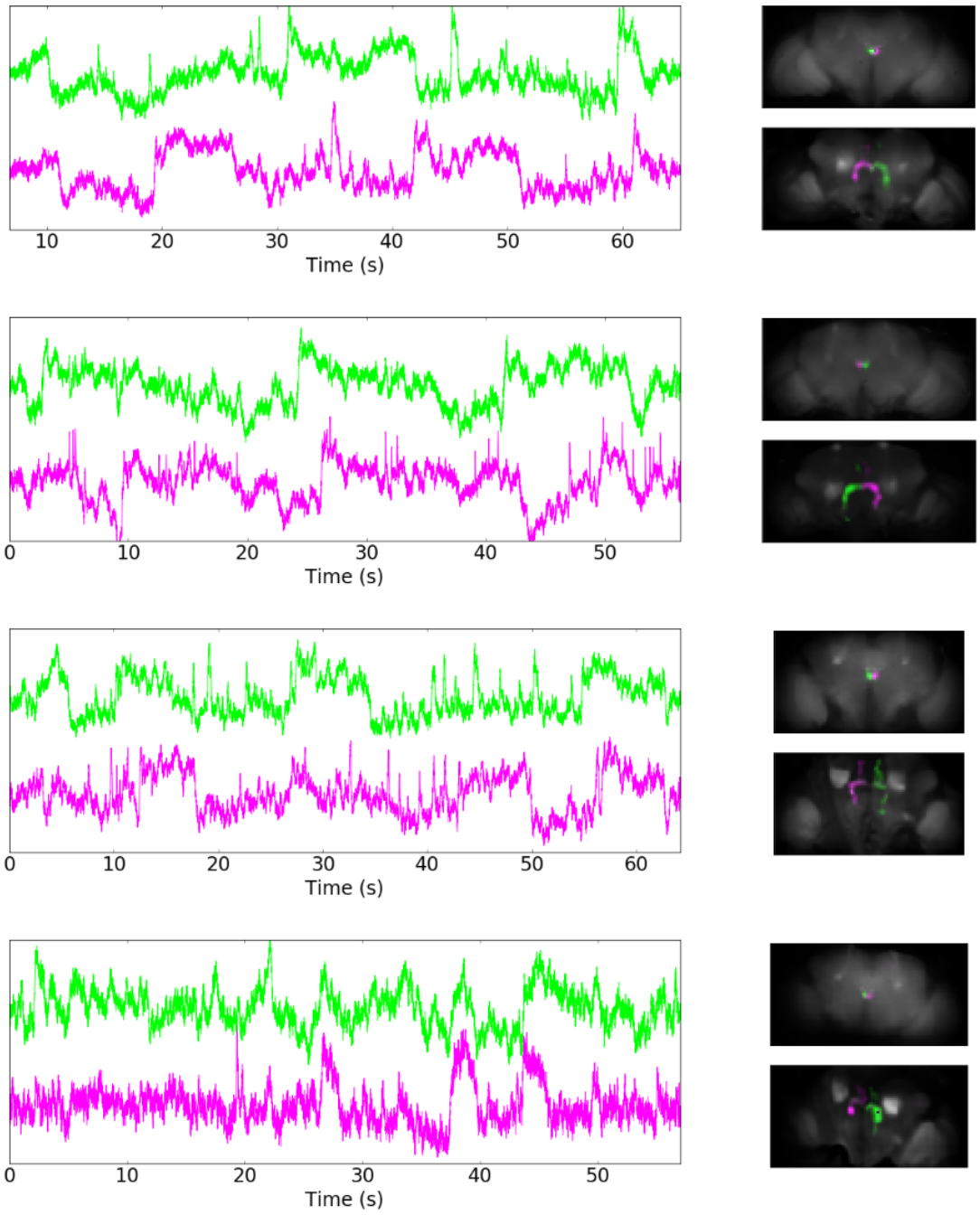
Figure 8: Spontaneous flip-flop activity of components in a nodulus and the contralateral part of the protocerebral bridge. These components are detected in all four flies studied (genotype: UAS_ArcLight, and from top to bottom: nsyb-gal4, nsyb-gal4, Cha-gal4 and GMR-gal4, nsyb-gal4).